

## Research Article

# Cu(I) Modification during $\gamma$ -Fe<sub>2</sub>O<sub>3</sub> Nanoparticles Synthesis and Subsequent Characterization

Hong Mao,<sup>1</sup> Xiaoyan Qiu,<sup>1</sup> Decai Li,<sup>2</sup> Yueqiang Lin,<sup>1</sup> Xiaodong Liu,<sup>1</sup> and Jian Li<sup>1</sup>

<sup>1</sup>School of Physical Science and Technology, Southwest University, Chongqing 400715, China

<sup>2</sup>School of Mechanical and Control Engineering, Beijing Jiaotong University, Beijing 100044, China

Correspondence should be addressed to Jian Li; [aizhong@swu.edu.cn](mailto:aizhong@swu.edu.cn)

Received 12 September 2015; Accepted 23 November 2015

Academic Editor: Josefina Pons

Copyright © 2015 Hong Mao et al. This is an open access article distributed under the Creative Commons Attribution License, which permits unrestricted use, distribution, and reproduction in any medium, provided the original work is properly cited.

During the synthesis of the  $\gamma$ -Fe<sub>2</sub>O<sub>3</sub> nanoparticles via the chemically induced transition method, Cu(I) modification has been attempted by adding CuCl/NaOH to the treatment solution. The experimental results showed that, under the condition of a NaOH content equal to 0.04 moles, when the content of CuCl is as low as  $1.25 \times 10^{-3}$  or  $2.50 \times 10^{-3}$  moles, the products are single  $\gamma$ -Fe<sub>2</sub>O<sub>3</sub>/Cu(I)FeO<sub>2</sub>/FeCl<sub>3</sub>·6H<sub>2</sub>O composite nanoparticles, whereas when the content of CuCl is higher,  $5 \times 10^{-2}$  moles, the product is a mixture consisting of  $\gamma$ -Fe<sub>2</sub>O<sub>3</sub>/Cu(I)FeO<sub>2</sub>/FeCl<sub>3</sub>·6H<sub>2</sub>O nanoparticles and Cu(II)(OH)Cl nanoparticles. For the  $\gamma$ -Fe<sub>2</sub>O<sub>3</sub>/Cu(I)FeO<sub>2</sub>/FeCl<sub>3</sub>·6H<sub>2</sub>O composite nanoparticles, the Cu(I)FeO<sub>2</sub> interface layer is not thick enough to form one unit cell, but it can modify the formation of a FeCl<sub>3</sub>·6H<sub>2</sub>O surface layer and the effective magnetization of the  $\gamma$ -Fe<sub>2</sub>O<sub>3</sub> core.

## 1. Introduction

By definition, nanomaterials have one or more dimensions in the nanometer scale range (<100 nm) and consequently show novel properties when compared to bulk materials [1]. A nanocomposite is a material composed of two or more phases. Nanoparticles are typically defined as solids measuring less than 100 nm in all the three dimensions; composite nanoparticles are generally coatings in which the combination of different physical and chemical properties may lead to completely novel materials with modified properties [1, 2]. Significant research effort has shown that the surface modification of the particles can be easily accomplished in postsynthesis steps or during the synthesis, thereby providing the nanoparticles with additional functionalities [3]. Magnetic nanoparticles constitute an important class of functional materials and can be categorized, based on single or multiple materials, into simple and core/shell—or composite—nanoparticles, which are gaining increasing interest because of their novel properties and the numerous applications in many diverse fields [3–5]. Composite magnetic iron oxide nanoparticles have applications ranging from ferrofluids to separation science and technology [6–8].

Studies on nanoparticles have focused on the development of simple and effective methods for fabricating nanomaterials with controlled size and morphology and hence tailoring their properties [9]. Liquid-phase synthesis is often used to prepare inorganic nanoparticles [10]; the conventional aqueous synthesis of the  $\gamma$ -Fe<sub>2</sub>O<sub>3</sub> particles involves three or more steps [11, 12]. We have proposed a method to synthesize  $\gamma$ -Fe<sub>2</sub>O<sub>3</sub> nanoparticles by thermally treating the FeOOH/Mg(OH)<sub>2</sub> precursor in FeCl<sub>2</sub> treating solution [13, 14]. Through this method, known as chemically induced transition (CIT) method, FeOOH species were transformed into  $\gamma$ -Fe<sub>2</sub>O<sub>3</sub> nanocrystallites by dehydration and Mg(OH)<sub>2</sub> was dissolved to assist the precipitation of the nanoparticles. Besides, the Fe<sup>2+</sup> ions in the FeCl<sub>2</sub> solution were oxidized to Fe<sup>3+</sup> to form a FeCl<sub>3</sub>·6H<sub>2</sub>O coating on the  $\gamma$ -Fe<sub>2</sub>O<sub>3</sub> nanocrystallites [14]. During the synthesis of the  $\gamma$ -Fe<sub>2</sub>O<sub>3</sub> nanoparticles, the surface modification was performed by adding a salt solution composed of metal ions with a valency of two, such as Zn(II)Cl<sub>2</sub> [15, 16] and Co(II)(NO<sub>3</sub>)<sub>2</sub> [17], to fabricate Zn(II)Fe<sub>2</sub>O<sub>4</sub> and Co(II)Fe<sub>2</sub>O<sub>4</sub> epitaxial layers, respectively, on the  $\gamma$ -Fe<sub>2</sub>O<sub>3</sub> crystallites. Additional NaOH can enhance these modifications to produce more ZnFe<sub>2</sub>O<sub>4</sub> or CoFe<sub>2</sub>O<sub>4</sub>. In this work, a surface modification

using metal ions with a valency of one is attempted by adding Cu(I)Cl/NaOH to the FeCl<sub>2</sub> treating solution, and the as-prepared products were characterized using multiple techniques. Accordingly, the features of the Cu(I)-modified  $\gamma$ -Fe<sub>2</sub>O<sub>3</sub> nanoparticles were investigated.

## 2. Materials and Methods

**2.1. Chemicals.** Ferric chloride (FeCl<sub>3</sub>), magnesium nitrate (Mg(NO<sub>3</sub>)<sub>2</sub>), ferrous chloride (FeCl<sub>2</sub>), cuprous chloride (CuCl), and sodium hydroxide (NaOH) were of analytical grade, and all other chemicals were used as received without further purification. Distilled water was used throughout the experiments.

**2.2. Preparation.** The preparation of Cu(I)-modified  $\gamma$ -Fe<sub>2</sub>O<sub>3</sub> nanoparticles by the so-called chemically induced transition method can be divided into two steps. First, the FeOOH/Mg(OH)<sub>2</sub> precursor was synthesized by coprecipitation, as described in detail elsewhere [13]. Second, 5 g of the precursor was added to a boiling FeCl<sub>2</sub> treating solution (0.25 M, 400 mL) and kept boiling under reflux for 20 min. Then, both CuCl solution (50 mL), with a varying concentration, and NaOH solution (2 M, 20 mL) were added simultaneously to the solution, and the resulting mixture was boiled continuously for 10 min. After cooling naturally to room temperature, the products precipitated from the solution; subsequently, they were washed with acetone and allowed to dry. The concentrations of the CuCl solutions were 0.025, 0.050, and 1.000 M, corresponding to samples (1), (2), and (3), respectively. For comparison, unmodified particles were also prepared by adding the precursor to the FeCl<sub>2</sub> solution and boiling for 30 min, producing sample (0).

**2.3. Characterization.** The bulk chemical compositions of the as-prepared products were obtained by energy dispersive X-ray spectroscopy (EDS, Quanta-200). The morphologies were observed by transmission electron microscopy (TEM, G20ST). The crystal properties were analyzed by high-resolution TEM (HRTEM, JEM-2100F) and X-ray diffractometry (XRD, D/Max-RC). The surface chemical compositions were determined by X-ray photoelectron spectroscopy (XPS, ESCALAB250Xi). The specific magnetization curves were measured at room temperature by vibrating sample magnetometry (VSM, HH-15).

## 3. Results and Discussion

**3.1. Results.** The EDS measurements revealed that samples (1), (2), and (3) contained not only O, Fe, and Cl and no Mg or Na—as sample (0)—but also Cu. Figure 1 shows the EDS spectra. The atomic percentages of the Fe, Cl, and Cu elements ( $a_i$  values), listed in Table 1, show that the amount of Cu increases from sample (1) to sample (3).

Typical TEM images are shown in Figure 2. All the samples are made of approximately spherical nanoparticles involving hexagonal particles. The size of the nanoparticles for both samples (1) and (2) is clearly larger than that of the

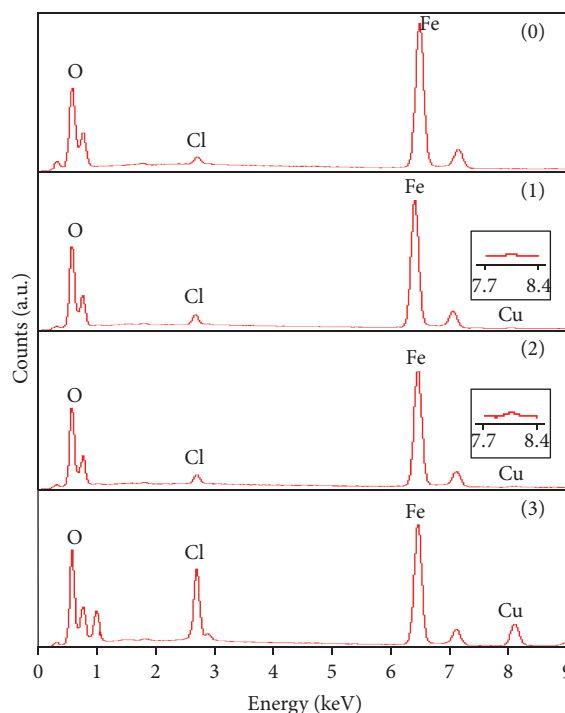


FIGURE 1: Energy dispersive X-ray spectroscopy (EDS) spectra of samples (0), (1), (2), and (3).

unmodified sample (0). Additionally, sample (3) contained two kinds of particles, larger size and smaller size, as the arrows marked with “A” and “B,” respectively, indicate.

The HRTEM revealed these particles to be small crystallites. Figure 3 is a typical HRTEM image of sample (2), which shows that the interlaced lattice fringes of two sets of planes have the same spacing of approximately 0.29 nm. As shown by the XRD spectra in Figure 4, the modified samples can be divided into two types, with samples (1) and (2) belonging to the same type and sample (3) showing notable differences. Similar to the unmodified sample (0), samples (1) and (2) predominantly possess a ferrite-like spinel structure with the features of  $\gamma$ -Fe<sub>2</sub>O<sub>3</sub> (JCPDS card number 39-1346). Sample (3) clearly contained  $\gamma$ -Fe<sub>2</sub>O<sub>3</sub> and Cu(II)(OH)Cl (JCPDS card number 23-1063).

For samples (1), (2), and (3), the XPS results confirmed the presence of the same chemical elements as determined by EDS. The quantitative results for the Fe, Cl, and Cu elements are listed in Table 1. Figure 5 shows the O 1s, Fe 2p<sub>3/2</sub>, Cl 2p, and Cu 2p spectra for samples (1) to (3). Similar to the XRD results, the XPS spectra can also be divided into two categories and are analyzed as follows.

Both samples (1) and (2) have the same XPS spectral structure. Their O 1s spectra exhibited two peaks: the P1 peak at approximately 529.5 eV can be attributed to Fe<sub>2</sub>O<sub>3</sub>, and the P2 peak at approximately 532.2 eV is due to molecular H<sub>2</sub>O [19]. The Cl 2p<sub>3/2</sub> peak at approximately 198.7 eV corresponds to Cl 2p<sub>3/2</sub> in FeCl<sub>3</sub> (199 eV), which is in good agreement with the probable presence of FeCl<sub>3</sub>·6H<sub>2</sub>O, as unmodified sample [14]. Thus, the Fe 2p<sub>3/2</sub> peak at ~711.2 eV resulted from both

TABLE 1: Atomic percentages of Fe, Cl, and Cu from energy dispersive X-ray spectroscopy (EDS) and X-ray photoelectron spectroscopy (XPS) measurements for samples (1), (2), and (3).

Sample	EDS				XPS			
	Fe	Cl	Cu	Cu/Cl	Fe	Cl	Cu	Cu/Cl
(0)	97.28	2.72						
(1)	95.19	4.04	0.77	0.19	63.06	32.64	4.30	0.13
(2)	94.73	3.93	1.34	0.34	56.24	38.58	5.18	0.13
(3)	60.99	19.03	19.98	1.05	35.18	51.13	13.69	0.27

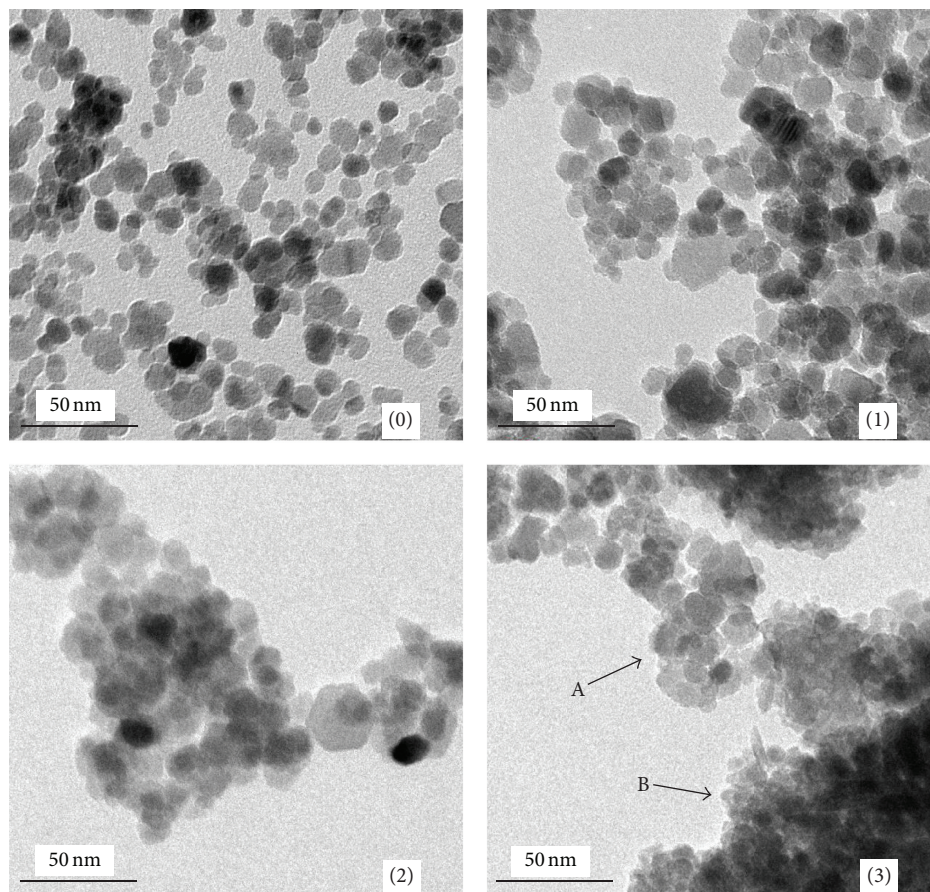


FIGURE 2: Typical transmission electron microscopy (TEM) images of samples (0), (1), (2), and (3).

$\gamma$ - $\text{Fe}_2\text{O}_3$  and  $\text{FeCl}_3$ . The  $\text{Cu } 2p_{3/2}$  peak at  $\sim 932.0$  eV clearly corresponds to  $\text{Cu(I)FeO}_2$  ( $\text{Cu } 2p_{3/2}$  peaks at 932.6 eV), rather than  $\text{Cu(II)Fe}_2\text{O}_4$  ( $\text{Cu } 2p_{3/2}$  peaks at 933.7 eV) [20]. The binding energy data of both samples (1) and (2) are listed in Table 2(a). For sample (3), the O 1s and Fe  $2p_{3/2}$  spectra are similar to those of samples (1) and (2). The Cl 2p spectrum exhibited two peaks, and the P1 peak (198.59 eV) could correspond to  $\text{FeCl}_3$ . Therefore, the Fe-containing compounds in sample (3) also consisted of both  $\gamma$ - $\text{Fe}_2\text{O}_3$  and  $\text{FeCl}_3 \cdot 6\text{H}_2\text{O}$ . The spectrum of Cu 2p of sample (3) has a more complicated structure than the spectra of both samples (1) and (2). It is known that the filled 3d shell of  $\text{Cu}^+$  could prevent the ligand-metal charge transfer shake-up transition from occurring, so that one major difference between Cu(I)

oxide and Cu(II) oxide is the satellite structure on the high energy side of the copper core lined in Cu(II) oxide [20]. The XRD analysis clearly determined that sample (3) contained  $\text{Cu(OH)Cl}$ ; thus, besides the P0 peak corresponding to the Cu peaks present in samples (1) and (2) and attributed to  $\text{Cu } 2p_{3/2}$  in  $\text{CuFeO}_2$ , the  $\text{P0}'$  peak could originate from  $\text{Cu } 2p_{1/2}$  in  $\text{CuFeO}_2$  and other peaks could result from  $\text{Cu(OH)Cl}$ . The Cu spectrum of sample (3) shows a pronounced shake-up satellite (SAT) structure, which is similar to the structure of Cu 2p in  $\text{CuCl}_2$  [18]. Furthermore, as the Cl 2p spectrum of  $\text{CuCl}_2$  has two distinguishable Cl  $2p_{1/2}$  and Cl  $2p_{3/2}$  peaks [18], the spectrum of  $\text{Cu(OH)Cl}$  could contain a contribution from both Cl  $2p_{1/2}$  and Cl  $2p_{3/2}$ , explaining the two peaks exhibited by the Cl spectrum of sample (3). The binding

TABLE 2: Binding energies (eV) from X-ray photoelectron spectroscopy (XPS) spectra for samples (1), (2), and (3).

(a) For samples (1) and (2)						
	O 1s		Fe 2p <sub>3/2</sub>	Cl 2p <sub>3/2</sub>	Cu 2p <sub>3/2</sub>	
Sample (1)	529.79 (P1);	532.39 (P2)	711.39	198.59	932.09	
Sample (2)	529.29 (P1);	532.09 (P2)	711.09	198.79	931.99	
Fe <sub>2</sub> O <sub>3</sub>	529.6		710.7			
CuFeO <sub>2</sub>	?		?		932.6	
FeCl <sub>3</sub>			711.3	199.0		
H <sub>2</sub> O	532.8					
(b) For sample (3)						
	O 1s		Fe 2p <sub>3/2</sub>	Cl 2p <sub>3/2</sub>	Cu 2p <sub>3/2</sub>	Cu 2p <sub>1/2</sub>
Sample (3)	530.09 (P1);	532.49 (P2)	711.19	198.59 (P1)	932.59 (P0)	952.38 (P0')
Fe <sub>2</sub> O <sub>3</sub>	529.6		710.7			
CuFeO <sub>2</sub>	?		?		932.6	Δ
FeCl <sub>3</sub>			711.3	199.0		
H <sub>2</sub> O	532.8					
	Cl 2p <sub>3/2</sub>	Cl 2p <sub>1/2</sub>	Cu 2p <sub>3/2</sub>	STA	Cu 2p <sub>1/2</sub>	STA
Sample (3)	198.59 (P1)	200.09 (P2)	934.59 (P1)	943.50 (P2)	954.49 (P3)	962.50 (P4)
Cu(OH)Cl	Δ	Δ	Δ	Δ	Δ	Δ
CuCl <sub>2</sub>	199.1	200.7	935.7	943.2	955.3	964.0
				945.6		

Note: standard data for Fe<sub>2</sub>O<sub>3</sub>, CuFeO<sub>2</sub>, FeCl<sub>3</sub>, and H<sub>2</sub>O from the NIST X-ray Photoelectron Spectroscopy Database at <http://www.nist.gov>, in which no O 1s, Fe 2p<sub>3/2</sub>, and Cu 2p<sub>1/2</sub> data for CuFeO<sub>2</sub> and no Cu(OH)Cl data were provided. Standard data for CuCl<sub>2</sub> from [18]. The binding energy of both O 1s and Fe 2p<sub>3/2</sub> for CuFe<sub>2</sub>O could not be determined in the present investigation.

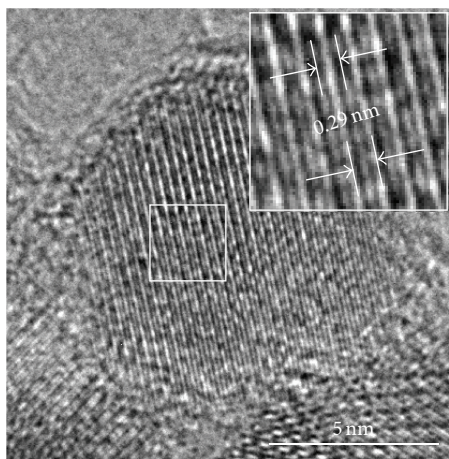


FIGURE 3: High-resolution transmission electron microscopy (HRTEM) image of a particle from sample (2).

energy data of sample (3) are listed in Table 2(b). As a comparison, the data of CuCl<sub>2</sub> are also listed in Table 2(b).

The specific magnetization curves of samples (0), (1), (2), and (3) in Figure 6 show that the samples exhibit a ferromagnetic behavior. Thus, the specific saturation magnetization,  $\sigma_s$ , can be estimated from a plot of  $\sigma$  versus  $1/H$  at high field [21]. For samples (0), (1), (2), and (3), the  $\sigma_s$  are 57.71, 66.59, 71.80, and 38.37 emu/g, respectively.

**3.2. Discussion.** According to the experimental results, every sample modified by CuCl/NaOH contained same  $\gamma$ -Fe<sub>2</sub>O<sub>3</sub> phase as the unmodified sample (0). Also, the modified samples have Cu-containing compounds. This result indicates that the precursor first transformed into  $\gamma$ -Fe<sub>2</sub>O<sub>3</sub> crystallites in the FeCl<sub>2</sub> treating solution and, then, following the addition of CuCl/NaOH, the Cu-containing compounds were formed. Under an additional specific content of NaOH equal to  $4 \times 10^{-2}$  moles (20 mL, 2 M), the composition of the as-prepared products depended on the content of additional CuCl. For lower contents of CuCl— $1.25 \times 10^{-3}$  moles (50 mL, 0.025 M) and  $2.50 \times 10^{-3}$  moles (50 mL, 0.050 M), that is, samples (1) and (2), respectively—the Cu-containing compound is Cu(I)FeO<sub>2</sub>, whereas when the content of CuCl is higher— $5.00 \times 10^{-2}$  moles (50 mL, 1.000 M), that is, sample (3)—the product exhibits two different Cu-containing compounds: Cu(I)FeO<sub>2</sub> and Cu(II)(OH)Cl. These results reveal that, by adding CuCl/Na(OH) to the treating solution, the oxidation of the Cu<sup>+</sup> ions and the formation of the Cu-containing compounds could depend on the concentration of CuCl under a certain content of NaOH. At low CuCl concentration, all the Cu<sup>+</sup> ions formed Cu(I)FeO<sub>2</sub> and no Cu(II) compound was created, whereas, at higher CuCl concentration, part of the Cu<sup>+</sup> ions formed Cu(I)FeO<sub>2</sub>, and the remaining Cu<sup>+</sup> ions were oxidized to Cu<sup>2+</sup> ions to produce Cu(II)(OH)Cl. The formation of Cu(OH)Cl rather than CuFe<sub>2</sub>O<sub>4</sub> could be due to a reason similar to that behind the formation of Cu<sub>2</sub>(OH)<sub>3</sub>NO<sub>3</sub>, where Cu<sup>2+</sup> does not coprecipitate with Fe<sup>3+</sup> as the pH of the reaction is too low [22].

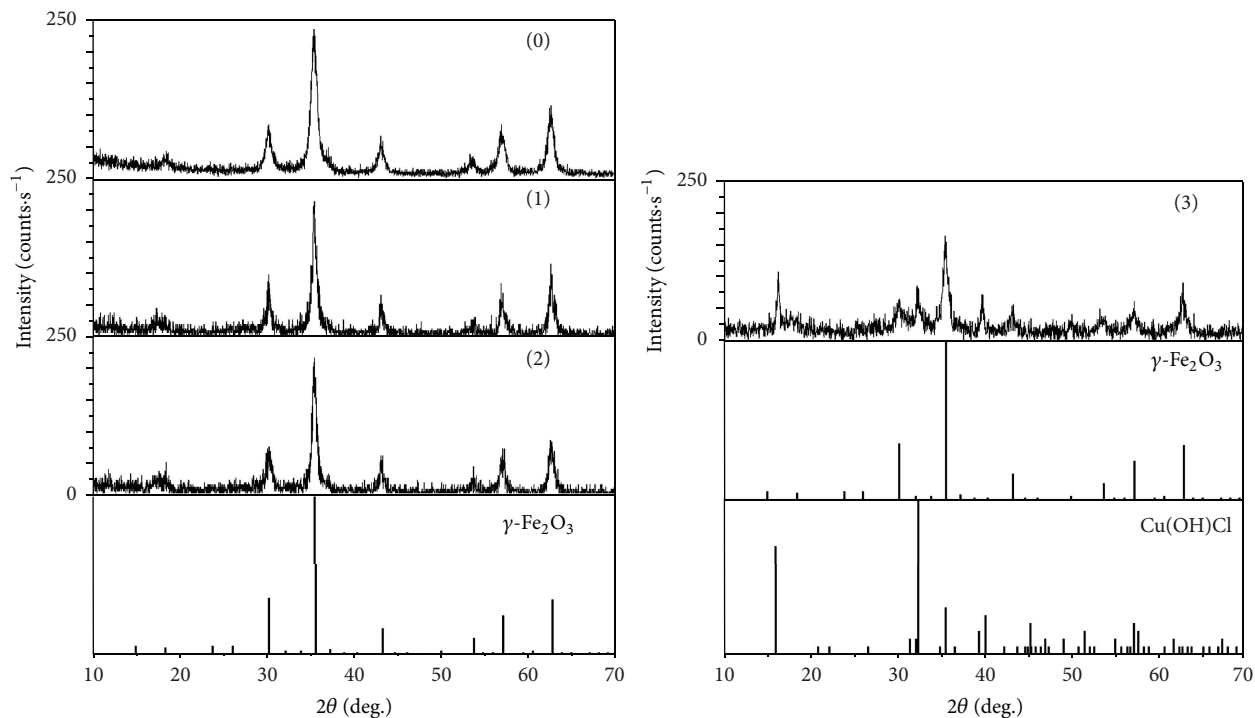


FIGURE 4: X-ray diffractometry (XRD) spectra of samples (0), (1), (2), and (3).

For the unmodified sample (0), it is known that  $\text{FeCl}_3 \cdot 6\text{H}_2\text{O}$  forms on the  $\gamma\text{-Fe}_2\text{O}_3$  crystallites [14]. XPS results revealed the presence of  $\text{FeCl}_3 \cdot 6\text{H}_2\text{O}$  in the modified samples (1), (2), and (3). For both samples (1) and (2), based on the  $\gamma\text{-Fe}_2\text{O}_3$ ,  $\text{Cu(I)FeO}_2$ , and  $\text{FeCl}_3 \cdot 6\text{H}_2\text{O}$  phases, the nanoparticles contained  $\gamma\text{-Fe}_2\text{O}_3$  and  $\text{FeCl}_3 \cdot 6\text{H}_2\text{O}$ , as confirmed by the lattice fringes of the two sets of planes observed in the HRTEM images, which precisely correspond to the (220) plane of  $\gamma\text{-Fe}_2\text{O}_3$  (spacing of 0.2953 nm) and (002) plane of  $\text{FeCl}_3 \cdot 6\text{H}_2\text{O}$  (spacing of 0.2927 nm), respectively. The  $\text{Cu(I)FeO}_2$  could be an intermediate layer formed between the  $\gamma\text{-Fe}_2\text{O}_3$  core and the  $\text{FeCl}_3 \cdot 6\text{H}_2\text{O}$  surface layer, as the ratio of Cu to Cl obtained from the XPS measurement is lower than that obtained from the EDS measurement. As a consequence, a schematic model of the particle structure of both samples (1) and (2) is shown in Figure 7. This inference can be explained as follows.

Notably, the collection depth of the signal in the EDS analysis largely exceeds the dimensions of the nanoparticles, whereas the signal collection depth in the XPS experiment is  $\sim 3\lambda$ , where  $\lambda = 1.24$  nm and 1.51 nm for Fe 2p and Cu 2p electrons, respectively [23, 24]. After statistical analysis [25], the TEM results revealed that the size of the particles of both samples (1) and (2) followed a lognormal distribution similar to that of sample (0). Their median diameter  $d_g$  and standard deviation  $\ln \sigma_g$  are listed in Table 3. Consequently, the average size of the particles  $\langle d \rangle$  is calculated by the formula  $\langle d \rangle = \exp[\ln d_g + 0.5 \ln^2 \sigma_g]$  [25], and the results show the size of samples (1) and (2) larger than 11 nm, as also listed in Table 3. Thus, for the nanoparticles in samples (1) and (2), the EDS results reflected the average ratio of the elements

TABLE 3: Size data measured from the transmission electron microscopy (TEM) images for samples (0), (1), and (2).

Sample	$d_g$ (nm)	$\ln \sigma_g$	$\langle d \rangle$ (nm)
(0)	10.24	0.36	10.93
(1)	11.64	0.29	12.14
(2)	11.03	0.28	11.47

in the nanoparticles, whereas the XPS results reflected the ratio of the elements near the nanoparticle surface. Therefore, for the nanoparticles having a multiple layer structure, as shown in Figure 7, as the depth of the XPS detection is smaller than the radius of the particles (as  $\langle d \rangle / 2$ ), the ratio of the elements in the internal layer to the elements in the outer layer, from XPS measurement, is lower than the average ratio in the total nanoparticle measured by EDS. For samples (1) and (2), the experimental results (see Table 1) show that the ratio of Cu to Cl from XPS measurements is far lower than that obtained from EDS measurements. Accordingly, for samples (1) and (2), the  $\text{Cu(I)FeO}_2$  grows between the  $\gamma\text{-Fe}_2\text{O}_3$  core and the  $\text{FeCl}_3 \cdot 6\text{H}_2\text{O}$  surface layer to form  $\gamma\text{-Fe}_2\text{O}_3/\text{Cu(I)FeO}_2/\text{FeCl}_3 \cdot 6\text{H}_2\text{O}$  composite nanoparticles.

Furthermore, sample (3) exhibited strong diffraction peaks of  $\text{Cu(II)(OH)Cl}$  in the XRD spectra. Therefore, sample (3) is a mixture of  $\gamma\text{-Fe}_2\text{O}_3/\text{Cu(I)FeO}_2/\text{FeCl}_3 \cdot 6\text{H}_2\text{O}$  nanoparticles and  $\text{Cu(II)(OH)Cl}$  nanoparticles, which may correspond to the larger and smaller particles, respectively, observed in the TEM image.

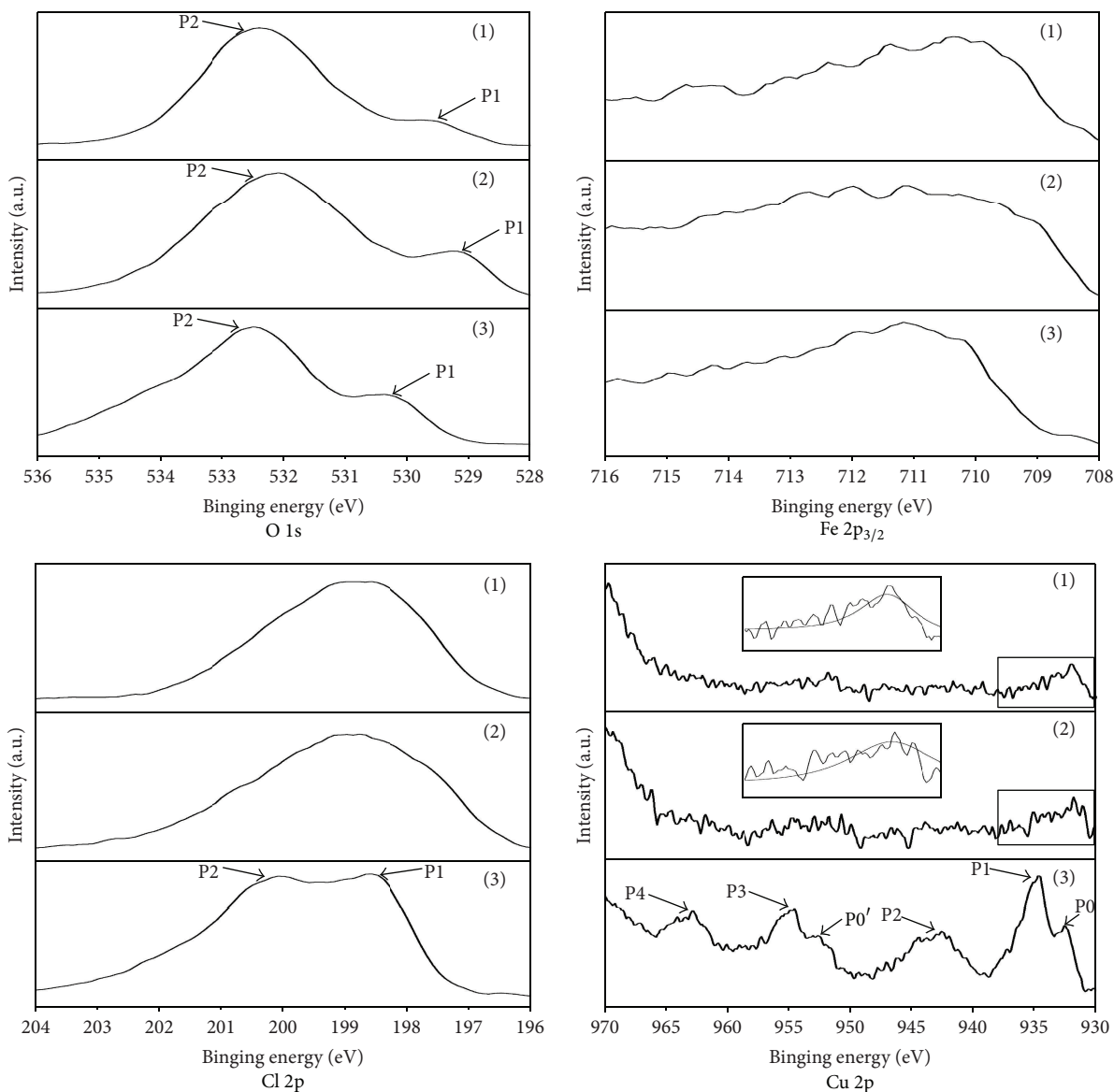


FIGURE 5: X-ray photoelectron spectroscopy (XPS) spectra of samples (1), (2), and (3), showing O 1s, Fe 2p<sub>3/2</sub>, Cl 2p, and Cu 2p.

For sample (0), based on  $\gamma$ -Fe<sub>2</sub>O<sub>3</sub>/FeCl<sub>3</sub>·6H<sub>2</sub>O nanoparticles, and samples (1) and (2), based on  $\gamma$ -Fe<sub>2</sub>O<sub>3</sub>/Cu(I)FeO<sub>2</sub>/FeCl<sub>3</sub>·6H<sub>2</sub>O nanoparticles, the molar percentages of the  $\gamma$ -Fe<sub>2</sub>O<sub>3</sub> phase,  $y_\gamma$ , Cu(I)FeO<sub>2</sub> phase,  $y_{\text{Cu-Fe}}$ , and FeCl<sub>3</sub>·6H<sub>2</sub>O phase,  $y_{\text{Fe-Cl}}$ , can be estimated by

$$y_\gamma = \frac{(a_{\text{Fe}} - a_{\text{Cu}} - a_{\text{Cl}}/3)/2}{(a_{\text{Fe}} - a_{\text{Cu}} - a_{\text{Cl}}/3)/2 + a_{\text{Cu}} + a_{\text{Cl}}/3} \times 100,$$

$$y_{\text{Cu-Fe}} = \frac{a_{\text{Cu}}}{(a_{\text{Fe}} - a_{\text{Cu}} - a_{\text{Cl}}/3)/2 + a_{\text{Cu}} + a_{\text{Cl}}/3} \times 100, \quad (1)$$

$$y_{\text{Cl-Fe}} = \frac{a_{\text{Cl}}/3}{(a_{\text{Fe}} - a_{\text{Cu}} - a_{\text{Cl}}/3)/2 + a_{\text{Cu}} + a_{\text{Cl}}/3} \times 100,$$

where  $a_{\text{Fe}}$ ,  $a_{\text{Cu}}$ , and  $a_{\text{Cl}}$  are the atomic percentages of Fe, Cu, and Cl, respectively, and  $a_{\text{Cu}}$  is equal to zero for sample (0).

Thus, the molar percentages of every phase in samples (0), (1), and (2) can be obtained from the values of  $a_{\text{Fe}}$ ,  $a_{\text{Cu}}$ , and  $a_{\text{Cl}}$  as measured by EDS (see Table 1). As a consequence, the mass percentages of these phases can be derived from

$$z_i = \frac{y_i A_i}{\sum y_i A_i} \times 100, \quad (2)$$

where  $y_i$  is the molar percentage and  $A_i$  is the molar mass of the  $i$  phase. Accordingly, the mass percentages of each phase in samples (0), (1), and (2) were calculated from the values of  $y_i$  and the molar masses of  $\gamma$ -Fe<sub>2</sub>O<sub>3</sub>, Cu(I)FeO<sub>2</sub>, and FeCl<sub>3</sub>·6H<sub>2</sub>O. The values of both  $y_i$  and  $z_i$  are listed in Table 4.

TABLE 4: Molar percentages  $y_i$  and mass percentages  $z_i$  of the phases for samples (0), (1), and (2).

Sample	$y_i$ (%)			$z_i$ (%)		
	$\gamma\text{-Fe}_2\text{O}_3$	$\text{Cu(I)FeO}_2$	$\text{FeCl}_3\cdot 6\text{H}_2\text{O}$	$\gamma\text{-Fe}_2\text{O}_3$	$\text{Cu(I)FeO}_2$	$\text{FeCl}_3\cdot 6\text{H}_2\text{O}$
(0)	98.15		1.85	96.91		3.09
(1)	96.56	1.58	2.77	93.93	1.47	4.60
(2)	94.56	2.75	2.69	92.96	2.56	4.48

TABLE 5: Volume percentages of phases  $\phi_i$ , average density ( $\text{g}/\text{cm}^3$ )  $\langle\rho\rangle$ , and saturation magnetization ( $\text{emu}/\text{cm}^3$ )  $M_s$  for samples (0), (1), and (2).

Sample	$\phi_i$ (%)			$\langle\rho\rangle$	$M_s$
	$\gamma\text{-Fe}_2\text{O}_3$	$\text{Cu(I)FeO}_2$	$\text{FeCl}_3\cdot 6\text{H}_2\text{O}$		
(0)	92.19		7.81	4.66	268.93
(1)	87.35	1.24	11.41	4.56	303.65
(2)	86.72	2.16	11.11	4.57	328.13

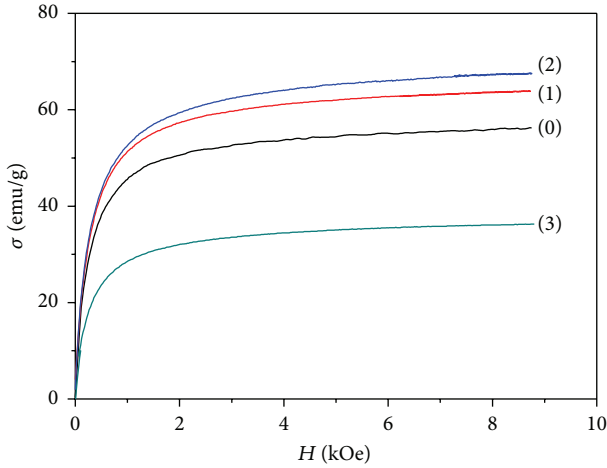


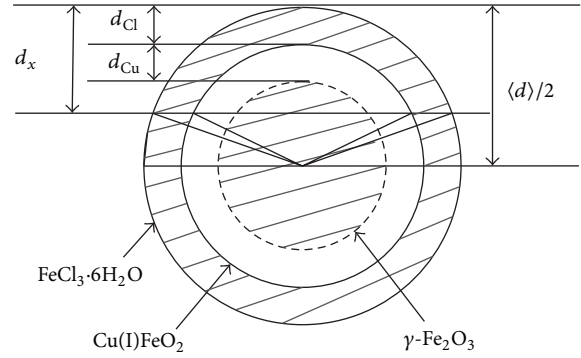
FIGURE 6: Specific magnetization curves of samples (0), (1), (2), and (3).

For samples (1) and (2), the specific magnetization  $\sigma$  can be described by

$$\sigma = \frac{(z_\gamma \sigma_\gamma + z_{\text{Cu-Fe}} \sigma_{\text{Cu-Fe}} + z_{\text{Fe-Cl}} \sigma_{\text{Fe-Cl}})}{100}, \quad (3)$$

where  $\sigma_\gamma$ ,  $\sigma_{\text{Cu-Fe}}$ , and  $\sigma_{\text{Fe-Cl}}$  are the specific magnetization of the  $\gamma\text{-Fe}_2\text{O}_3$ ,  $\text{Cu(I)FeO}_2$ , and  $\text{FeCl}_3\cdot 6\text{H}_2\text{O}$  phase, respectively, and  $z_i/100$  is the mass fraction of the  $i$  phase. As  $\gamma\text{-Fe}_2\text{O}_3$  and  $\text{Cu(I)FeO}_2$  are ferrimagnetic and  $\text{FeCl}_3\cdot 6\text{H}_2\text{O}$  is paramagnetic, the specific magnetization of both samples (1) and (2) results mainly from the mass percentages of the ferrimagnetic phase,  $z_f = z_r + z_{\text{Cu-Fe}}$ . From the results listed in Table 4,  $z_f = 95.40$  for sample (1) and  $z_f = 95.52$  for sample (2). Thus, the specific magnetization of sample (1) is slightly less than that of sample (2). In addition, sample (3) contained  $\text{Cu(II)(OH)Cl}$  particles, so the specific magnetization of sample (3) is lower than that of both samples (1) and (2).

The magnetization (moment per unit volume)  $M$  is an important parameter used to characterize magnetic materials. For a particle system, the magnetization can be obtained

FIGURE 7: Schematic diagram of the nanoparticles structures of samples (1) and (2);  $d_x$  indicates the depth detected by XPS;  $d_{\text{Cl}}$  is the thickness of  $\text{FeCl}_3\cdot 6\text{H}_2\text{O}$ ;  $d_{\text{Cu}}$  is the thickness of  $\text{Cu(I)FeO}_2$ .

generally from  $M = \sigma \cdot \rho$ , where  $\sigma$  is the specific magnetization (moment per unit mass) and  $\rho$  is the density of the material. For composite nanoparticles containing many phases with different densities, the density of the particles should be taken as the average density  $\langle\rho\rangle$ , which can be derived from

$$\langle\rho\rangle = \sum \frac{\phi_i \rho_i}{100}, \quad (4)$$

where  $\phi_i$  is volume percentage and  $\rho_i$  is density of the  $i$  phase. The  $\phi_i$  can be described as

$$\phi_i = \frac{z_i \rho_i}{\sum z_i \rho_i} \times 100. \quad (5)$$

Accordingly, the volume percentages  $\phi_i$  of the  $\gamma\text{-Fe}_2\text{O}_3$ ,  $\text{Cu(I)FeO}_2$ , and  $\text{FeCl}_3\cdot 6\text{H}_2\text{O}$  phases in samples (0), (1), and (2) can be calculated, and the average density  $\langle\rho\rangle$  for every sample can be derived. Therefore, the saturation magnetization  $M_s = \sigma_s \cdot \langle\rho\rangle$  can be obtained. These results,  $\phi_i$ ,  $\langle\rho\rangle$ , and  $M_s$  for samples (0), (1), and (2), are listed in Table 5.

For samples (1) and (2), the amount of  $\text{Cu(I)FeO}_2$  listed in Table 5 is so small that the thickness of the  $\text{Cu(I)FeO}_2$

in the  $\gamma\text{-Fe}_2\text{O}_3/\text{Cu(I)FeO}_2/\text{FeCl}_3\cdot 6\text{H}_2\text{O}$  nanoparticles is no more than one unit cell, and Cu(I) is not in the same state as in bulk Cu(I)FeO<sub>2</sub>; this case is similar to that of  $\gamma\text{-Fe}_2\text{O}_3$  nanoparticles having CoFe<sub>2</sub>O<sub>4</sub> layer less thick than one unit cell [26]. The presence of Cu(I)FeO<sub>2</sub> could modify the formation of FeCl<sub>3</sub>·6H<sub>2</sub>O and make the FeCl<sub>3</sub>·6H<sub>2</sub>O layer assume a three-dimensional (3D) oriented arrangement [27], so as to have a certain crystallized orientation relatively to the  $\gamma\text{-Fe}_2\text{O}_3$  crystallites. Therefore, both  $\gamma\text{-Fe}_2\text{O}_3$  and FeCl<sub>3</sub>·6H<sub>2</sub>O are identified in the HRTEM stripe images showing the two sets of planes. Also, the saturation magnetization of both the modified samples (1) and (2) is higher than that of the unmodified sample (0), although the ferrite volume percentages of the formers are lower than that of the latter. It is known that the spins close to the surface to be pinned by surfactant molecules, which cause anomalously large magnetic anisotropy, would result in the less apparent saturation magnetization of nanoparticles than that of the bulk [28]. Accordingly, it is judged that the Cu(I)FeO<sub>2</sub> thin layer in the  $\gamma\text{-Fe}_2\text{O}_3/\text{Cu(I)FeO}_2/\text{FeCl}_3\cdot 6\text{H}_2\text{O}$  nanoparticles may modify the magnetically silent “dead layer” [29], which existed at the interface between the  $\gamma\text{-Fe}_2\text{O}_3$  and FeCl<sub>3</sub>·6H<sub>2</sub>O phases of the  $\gamma\text{-Fe}_2\text{O}_3/\text{FeCl}_3\cdot 6\text{H}_2\text{O}$  nanoparticles of the unmodified sample (0) and did not provide any contribution to the effective magnetization.

#### 4. Conclusions

When the FeOOH/Mg(OH)<sub>2</sub> precursor was thermally treated in FeCl<sub>2</sub> solution, the Mg(OH)<sub>2</sub> dissolved, FeOOH transformed into  $\gamma\text{-Fe}_2\text{O}_3$  nanocrystallites, and Fe<sup>2+</sup> in the FeCl<sub>2</sub> treating solution was simultaneously oxidized to Fe<sup>3+</sup>. The nanocrystallites absorbed Fe<sup>3+</sup> and Cl<sup>-</sup> to form  $\gamma\text{-Fe}_2\text{O}_3/\text{FeCl}_3\cdot 6\text{H}_2\text{O}$  nanoparticles, in which the  $\gamma\text{-Fe}_2\text{O}_3$  core was coated with the FeCl<sub>3</sub>·6H<sub>2</sub>O layer. By adding Cu(I)Cl/NaOH to the FeCl<sub>2</sub> solution during the synthesis, the compositions of the as-prepared products can be modified. For a certain content of NaOH, 0.04 moles, using a low content of Cu(I)Cl ( $1.25 \times 10^{-3}$  moles or  $2.50 \times 10^{-3}$  moles), single Cu(I) modified composite nanoparticles can be prepared. The structure of such composite nanoparticles can be described as  $\gamma\text{-Fe}_2\text{O}_3/\text{Cu(I)FeO}_2/\text{FeCl}_3\cdot 6\text{H}_2\text{O}$  and consisted of three parts as follows:  $\gamma\text{-Fe}_2\text{O}_3$  core, a Cu(I)FeO<sub>2</sub> intermediate layer, and an outermost FeCl<sub>3</sub>·6H<sub>2</sub>O layer. For a higher content of CuCl,  $5 \times 10^{-2}$  moles, Cu<sup>+</sup> was partially oxidized to Cu<sup>2+</sup>, and the as-prepared product was a mixture of  $\gamma\text{-Fe}_2\text{O}_3/\text{Cu(I)FeO}_2/\text{FeCl}_3\cdot 6\text{H}_2\text{O}$  nanoparticles and Cu(II)(OH)Cl nanoparticles. The Cl and Cu spectra of Cu(OH)Cl measured by XPS have the same structure as those of CuCl<sub>2</sub>, and the binding energies of Cl 2p<sub>3/2</sub>, Cl 2p<sub>1/2</sub>, Cu 2p<sub>3/2</sub>, and Cu 2p<sub>1/2</sub> for the Cu(OH)Cl compound are approximately 198.6, 200.1, 934.6, and 954.5 eV, respectively.

For the  $\gamma\text{-Fe}_2\text{O}_3/\text{Cu(I)FeO}_2/\text{FeCl}_3\cdot 6\text{H}_2\text{O}$  composite nanoparticles, the average thickness of the Cu(I)FeO<sub>2</sub> layer is not enough to form one unit cell, and Cu(I) is not in the same state in bulk Cu(I)FeO<sub>2</sub>. The experimental results show that the Cu(I)FeO<sub>2</sub> intermediate layer could modify the formation of the FeCl<sub>3</sub>·6H<sub>2</sub>O layer to stimulate a 3D

oriented attachment of the layer relatively to the  $\gamma\text{-Fe}_2\text{O}_3$  crystallites; it may also modify the magnetic “dead layer” between the  $\gamma\text{-Fe}_2\text{O}_3$  core and FeCl<sub>3</sub>·6H<sub>2</sub>O surface layer to enhance the effective magnetization. Besides having high magnetization, such nanoparticles have an inert FeCl<sub>3</sub>·6H<sub>2</sub>O surface; therefore they could possess a relatively good chemical stability and can be used directly to synthesize ionic ferrofluids without ferric nitric treatment as the Massart method [30].

#### Conflict of Interests

The authors declare that there is no conflict of interests regarding the publication of this paper.

#### Acknowledgment


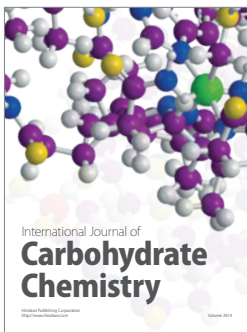
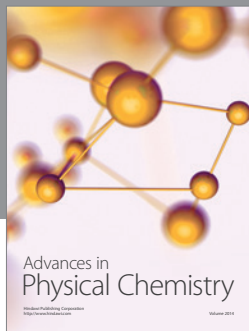
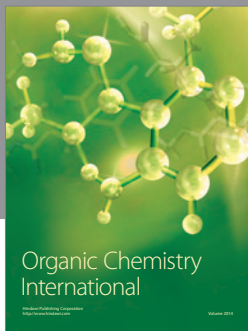
Financial support for this work was provided by the National Science Foundation of China (Grant no. 11274527, 5375039).

#### References

- [1] R. G. Chaudhuri and S. Paria, “Core/shell nanoparticles: classes, properties, synthesis mechanisms, characterization, and applications,” *Chemical Reviews*, vol. 112, no. 4, pp. 2373–2433, 2012.
- [2] D. V. Szabó and D. Vollath, “Nanocomposites from coated nanoparticles,” *Advanced Materials*, vol. 11, no. 15, pp. 1313–1316, 1999.
- [3] M. A. Willard, L. K. Kurihara, E. E. Carpenter, S. Calvin, and V. G. Harris, “Chemically prepared magnetic nanoparticles,” *International Materials Reviews*, vol. 49, no. 3-4, pp. 125–170, 2004.
- [4] T.-J. Yoon, H. Lee, H. Shao, and R. Weissleder, “Highly magnetic core-shell nanoparticles with a unique magnetization mechanism,” *Angewandte Chemie International Edition*, vol. 50, no. 20, pp. 4663–4666, 2011.
- [5] A. López-Ortega, M. Estrader, G. Salazar-Alvarez, A. G. Roca, and J. Nogués, “Applications of exchange coupled bi-magnetic hard/soft and soft/hard magnetic core/shell nanoparticles,” *Physics Reports*, vol. 553, pp. 1–32, 2015.
- [6] K. Kawaguchi, J. Jaworski, Y. Ishikawa, T. Sasaki, and N. Koshizaki, “Preparation of gold/iron-oxide composite nanoparticles by a unique laser process in water,” *Journal of Magnetism and Magnetic Materials*, vol. 310, no. 2, pp. 2369–2371, 2007.
- [7] H. Yuvaraj, M. H. Woo, E. J. Park, Y. T. Jeong, and K. T. Lim, “Polypyrrole/ $\gamma\text{-Fe}_2\text{O}_3$  magnetic nanocomposites synthesized in supercritical fluid,” *European Polymer Journal*, vol. 44, no. 3, pp. 637–644, 2008.
- [8] X. Xu, J. Wang, C. Yang, H. Wu, and F. Yang, “Sol-gel formation of  $\gamma\text{-Fe}_2\text{O}_3/\text{SiO}_2$  nanocomposites: effects of different iron raw material,” *Journal of Alloys and Compounds*, vol. 468, no. 1-2, pp. 414–420, 2009.
- [9] D. S. Mathew and R.-S. Juang, “An overview of the structure and magnetism of spinel ferrite nanoparticles and their synthesis in microemulsions,” *Chemical Engineering Journal*, vol. 129, no. 1–3, pp. 51–65, 2007.
- [10] B. L. Cushing, V. L. Kolesnichenko, and C. J. O’Connor, “Recent advances in the liquid-phase syntheses of inorganic nanoparticles,” *Chemical Reviews*, vol. 104, no. 9, pp. 3893–3946, 2004.



- [11] G. Salazar-Alvarez, J. Sort, A. Uheida et al., "Reversible post-synthesis tuning of the superparamagnetic blocking temperature of  $\gamma$ -Fe<sub>2</sub>O<sub>3</sub> nanoparticles by adsorption and desorption of Co(II) ions," *Journal of Materials Chemistry*, vol. 17, no. 4, pp. 322–328, 2007.
- [12] S. Asuha, S. Zhao, H. Y. Wu, L. Song, and O. Tegus, "One step synthesis of maghemite nanoparticles by direct thermal decomposition of Fe-urea complex and their properties," *Journal of Alloys and Compounds*, vol. 472, no. 1-2, pp. L23–L25, 2009.
- [13] B. C. Wen, J. Li, Y. Q. Lin et al., "A novel preparation method for  $\gamma$ -Fe<sub>2</sub>O<sub>3</sub> nanoparticles and their characterization," *Materials Chemistry and Physics*, vol. 128, no. 1-2, pp. 35–38, 2011.
- [14] H. Mao, J. Li, L. Chen et al., "Modification using additional NaOH for the preparation of  $\gamma$ -Fe<sub>2</sub>O<sub>3</sub> nanoparticles by chemically induced transition," *Micro & Nano Letters*, vol. 9, no. 11, pp. 782–786, 2014.
- [15] L. L. Chen, J. Li, Y. Q. Lin, X. D. Liu, L. H. Lin, and D. C. Li, "Preparation of composite nanoparticles of Fe–Zn bioxide using surface modification and their subsequent characterization," *IEEE Transactions on Magnetics*, vol. 50, no. 7, Article ID 2200106, 2014.
- [16] L. L. Chen, J. Li, Y. Q. Lin et al., "Preparation of  $\gamma$ -Fe<sub>2</sub>O<sub>3</sub>/ZnFe<sub>2</sub>O<sub>4</sub> nanoparticles by enhancement of surface modification with NaOH," *Chemistry Central Journal*, vol. 8, article 40, 2014.
- [17] J. M. Li, J. Li, L. L. Chen et al., "Characterization and magnetism of Co-modified  $\gamma$ -Fe<sub>2</sub>O<sub>3</sub> core-shell nanoparticles by enhancement using NaOH," *Journal of Magnetism and Magnetic Materials*, vol. 374, pp. 157–163, 2015.
- [18] W. Sesselmann and T. J. Chuang, "The interaction of chlorine with copper. I. Adsorption and surface reaction," *Surface Science*, vol. 176, no. 1-2, pp. 32–66, 1986.
- [19] N. Martenson, P.-A. Malmquist, S. Svensson et al., "Molecular and solid water, a comparative ESCA study," *New Journal of Chemistry*, vol. 1, pp. 191–195, 1977.
- [20] N. S. McIntyre and M. G. Cook, "X-ray photoelectron studies on some oxides and hydroxides of cobalt, nickel, and copper," *Analytical Chemistry*, vol. 47, no. 13, pp. 2208–2213, 1975.
- [21] R. Arulmurugan, G. Vaidyanathan, S. Sendhilnathan, and B. Jeyadevan, "Co-Zn ferrite nanoparticles for ferrofluid preparation: study on magnetic properties," *Physica B: Condensed Matter*, vol. 363, no. 1–4, pp. 225–231, 2005.
- [22] L. H. Lin, J. Li, Y. Q. Lin et al., "Preparation of ferrihydrite nanoclusters using hydrolysis enhanced by CuO and their subsequent characterisation," *Materials Research Innovations*, vol. 19, no. 2, pp. 118–124, 2015.
- [23] I. Srnová-Šloufová, B. Vlčková, Z. Bastl, and T. L. Haslett, "Bimetallic (Ag)Au nanoparticles prepared by the seed growth method: two-dimensional assembling, characterization by energy dispersive X-ray analysis, X-ray photoelectron spectroscopy, and surface enhanced raman spectroscopy, and proposed mechanism of growth," *Langmuir*, vol. 20, no. 8, pp. 3407–3415, 2004.
- [24] S. Tanuma, C. J. Powell, and D. R. Penn, "Calculation of electron mean free paths. II. Data for 27 elements over the 50–2000 eV range," *Surface and Interface Analysis*, vol. 17, no. 13, pp. 911–926, 1991.
- [25] C. G. Granqvist and R. A. Buhrman, "Ultrafine metal particles," *Journal of Applied Physics*, vol. 47, no. 5, pp. 2200–2219, 1976.
- [26] A. E. Berkowitz, F. E. Parker, E. L. Hall, and G. Podolsky, "Toward a model for Co-surface-treated Fe-oxides," *IEEE Transactions on Magnetics*, vol. 24, no. 6, pp. 2871–2873, 1988.
- [27] A. Narayanaswamy, H. Xu, N. Pradhan, and X. Peng, "Crystalline nanoflowers with different chemical compositions and physical properties grown by limited ligand protection," *Angewandte Chemie: International Edition*, vol. 45, no. 32, pp. 5361–5364, 2006.
- [28] M. Blanco-Mantecon and K. Ógrady, "Interaction and size effects in magnetic nanoparticles," *Journal of Magnetism and Magnetic Materials*, vol. 296, no. 2, pp. 124–133, 2006.
- [29] R. Frison, G. Cernuto, A. Cervellino et al., "Magnetite-maghemite nanoparticles in the 5–15 nm range: correlating the core-shell composition and the surface structure to the magnetic properties. A total scattering study," *Chemistry of Materials*, vol. 25, no. 23, pp. 4820–4827, 2013.
- [30] F. A. Tourinho, R. Franck, and R. Massart, "Aqueous ferrofluids based on manganese and cobalt ferrites," *Journal of Materials Science*, vol. 25, no. 7, pp. 3249–3254, 1990.



**Hindawi**

Submit your manuscripts at  
<http://www.hindawi.com>

